R. L. Weaver[1]

Yih-Hsing Pao
Fellow ASME

Department of Theoretical and Applied Mechanics, Cornell University, Ithaca, N.Y. 14853

Axisymmetric Elastic Waves Excited by a Point Source in a Plate

The response of an infinite elastic plate to dynamic loading is presented by the method of superposition of normal modes, a method particularly appropriate in the intermediate and far field. The method is compared with the method of integral transforms. Explicit expressions are given for the case of loading by a concentrated vertical step force. These expressions are evaluated numerically over a range of distances from 4 to 40 plate thicknesses. The numerical results are compared with qualitative stationary phase analyses and with the exact results of generalized ray theory.

1 Introduction

The propagation of waves in an infinite elastic plate has been studied since 1889 when Rayleigh [1] and Lamb [2] established the frequency equation for the dispersive waves based on the theory of elasticity. Since then there have been numerous contributions, notably those of Mindlin [3] on the dispersion relations and approximate theories and Miklowitz [4] on transient waves.

Most of the transient solutions are derived by applying double or triple integral transforms. The inverse transformation integrals are then evaluated either by the calculus of residues plus the method of stationary phase [5–7], or by the method of generalized rays [8–12]. As can be seen from the text by Miklowitz [4], the evaluation of these integrals in the first approach involves the understanding of the intricate behavior of dispersion relations for real as well as complex wave numbers. So far very little quantitative information about the wave motion at intermediate range (10–100 times the thickness of the plate from the source) or far range (100 times the thickness or longer) are available.

As for the application of the method of generalized rays, earlier results [8–10] were confined to epicentral response or wave motion very close to the source and epicenter. Only recently numerical results were reported for wave motion in near range (0 to 10 thickness from the source) [11, 12].

The theory of generalized rays is an exact method, as distinguished from the geometric ray theories. It becomes extremely cumbersome, though, for a receiver-source separation of greater than 10 plate thicknesses because a very large number of generalized ray integrals must be evaluated numerically. The paper by Ceranoglu and Pao [12] showed that 1586 ray integrals were calculated and summed at a range of six plate thicknesses over a duration of 10 transit times (one transit time is the time for the dilatational wave to cross the plate thickness once). Although all these ray integrals are assembled and calculated automatically by using one large computer code, it is not very practical when long time and far field results of wave motion are desired.

In this paper, we present another approach, the method of expansion in eigenfunctions, known also as the method of expansion in normal modes. This method, usually applied to finite bodies, is discussed in the Treatise (Sections 124-128) by Love [13]. A comprehensive treatment of the method can be found in the text (Section 5.17) by Eringen and Suhubi [14] and an application to finite bodies in the work of Reismann [15]. The method gives precisely the same expressions as can be obtained by integral transforms. The resulting expressions, as shown by numerical results in this paper, are particularly suitable for calculating intermediate and long range wave fields.

Since the concept of normal modes is well defined for a body bounded in all directions, we determine the normal modes of a thick, circular plate with a finite radius in free vibration in Sections 2 and 3, and formulate the solution of forced vibration of the plate by the method of normal mode expansion in Section 4. By letting the radius of the plate approach infinity, we then obtain, in Section 5, the solution for the transient waves in an infinite plate. Evaluation of the resulting integral expressions by the method of stationary phase is discussed in Section 7. Numerical evaluations are presented in Section 8. Throughout this paper, we consider only axially symmetric waves.

As discussed in Section 6, the method of normal mode expansion is easily applicable to surface forces as well as buried forces in a plate. Our interest in a solution for buried sources stems from developments in acoustic emission. With the advent of increasing sophistication in acoustic emission techniques, theoretical results for the dynamic response of a structure such as a large plate over a wide range of times and positions are needed to locate and to characterize the buried

[1] Present address: Department of Theoretical and Applied Mechanics, 216 Talbot Laboratory, 104 South Wright Street, University of Illinois, Urbana, Ill. 61801.

Contributed by the Applied Mechanics Division and presented at the Winter Annual Meeting, Phoenix, Ariz., November 14-19, 1982 of THE AMERICAN SOCIETY OF MECHANICAL ENGINEERS.

Discussion on this paper should be addressed to the Editorial Department, ASME, United Engineering Center, 345 East 47th Street, New York, N.Y. 10017, and will be accepted until two months after final publication of the paper itself in the JOURNAL OF APPLIED MECHANICS. Manuscript received by ASME Applied Mechanics Division, May, 1981; final revision, March, 1982. Paper No. 82-WA/APM-15.

Copies will be available until July, 1983.

Downloaded From: https://appliedmechanics.asmedigitalcollection.asme.org on 06/27/2019 Terms of Use: http://www.asme.org/about-asme/terms-of-use

Copyright © 1982 by ASME

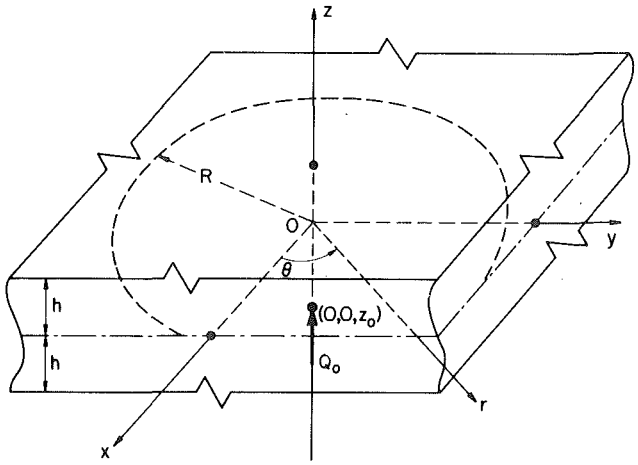

Fig. 1 Axisymmetric force in a thick plate

sources of emission. Of particular interest is the identification of those aspects of measured responses that are affected by the geometry of the plate, the source characteristics, or the receiver characteristics. This identification cannot be accomplished without a detailed theoretical analysis and numerical results.

2 Basic Equations

We consider an infinite elastic plate bounded by two parallel surfaces free of tractions at $z = \pm h$ (Fig. 1), $z = 0$ being the midplane of the plate. The circular cylindrical coordinates r, θ, z will be used to describe the response of the plate to an axisymmetric time-dependent force distribution.

The linear elastic wave equation is

$$\mathbf{L}(\mathbf{u}) \equiv (\lambda+\mu)\nabla(\nabla\cdot\mathbf{u}) + \mu\nabla^2\mathbf{u} = \rho\ddot{\mathbf{u}} - \mathbf{F}(\mathbf{x},t) \tag{2.1}$$

where $\mathbf{u}(\mathbf{x},t)$ is the time-dependent displacement at position $\mathbf{x}$, and $\mathbf{F}(\mathbf{x},t)$ is an externally applied body force density, usually taken equal to zero for $t \leq 0$. ρ is the mass density, and λ and μ the Lamé constants of the isotropic plate material, ρ, λ, and μ being assumed independent of $\mathbf{x}$ and t. The operator $\mathbf{L}$ is defined as $\mathbf{L} \equiv (\lambda+\mu)\nabla\nabla\cdot + \mu\nabla^2$. In the ensuing discussions we will consider only axisymmetric disturbances where all field quantities are independent of angular coordinate θ, and the θ component of displacement is zero.

The boundary conditions at the two parallel surfaces are

$$\sigma_{zr} = \sigma_{zz} = 0 \quad \text{at} \quad z = \pm h \tag{2.2}$$

In addition to these boundary conditions, there are also the initial conditions

$$\mathbf{u}(\mathbf{x},0) = \dot{\mathbf{u}}(\mathbf{x},0) = 0 \tag{2.3}$$

In many cases where the applied force is confined to the surfaces at $z = \pm h$, one may consider the equivalent problem obtained by setting $\mathbf{F}$ to zero but employing inhomogeneous time-dependent boundary conditions for the stresses at $z = \pm h$. As shown later, the case of surface loading can be treated as a special case of a general class of plate problems formulated by equations (2.1), (2.2), and (2.3).

Before considering the case of forced motion, we discuss first the free vibration of an elastic plate, $\mathbf{F} = 0$ in equation (2.1). We will investigate the simple harmonic motion of the plate, that is, solutions with time dependence $\exp(-i\omega t)$ for some real ω. This time-dependent factor will be suppressed throughout the following.

The problem of plane harmonic waves [1, 2] and circular-crest harmonic waves [16] in an infinite plate has been exhaustively examined [3, 17, 18]. We shall, however, repeat some of the results which are needed for ensuing discussions.

In addition to the boundary conditions at $z = \pm h$, we have the condition that $\mathbf{u}$ be regular at $\mathbf{r} = 0$. The boundary conditions at large r will be considered in Section 3. The harmonic solutions to equation (2.1) are then, for any κ

(1) Antisymmetric modes

$$\begin{aligned} u_r &= (B\sin\alpha z - C\beta\sin\beta z)\,\kappa J_0'(\kappa r) \\ u_z &= (B\alpha\cos\alpha z + C\kappa^2\cos\beta z)\,J_0(\kappa r), \end{aligned} \tag{2.4}$$

where

$$B/C = 2\kappa^2\beta\sin\beta h/(\kappa^2 - \beta^2)\sin\alpha h, \tag{2.5}$$

and ω satisfies

$$R_a(\omega,\kappa) \equiv (\kappa^2 - \beta^2)^2\sin\alpha h\cos\beta h + 4\alpha\beta\kappa^2\cos\alpha h\sin\beta h = 0. \tag{2.6a}$$

(2) Symmetric modes

$$\begin{aligned} u_r &= (A\cos\alpha z + D\beta\cos\beta z)\,\kappa J_0'(\kappa r) \\ u_z &= (-\alpha A\sin\alpha z + D\kappa^2\sin\beta z)\,J_0(\kappa r) \end{aligned} \tag{2.7}$$

where

$$A/D = -2\kappa^2\beta\cos\beta h/(\kappa^2 - \beta^2)\cos\alpha h \tag{2.8}$$

and ω satisfies

$$R_s(\omega,\kappa) \equiv (\kappa^2 - \beta^2)^2\cos\alpha h\sin\beta h + 4\alpha\beta\kappa^2\cos\beta h\sin\alpha h = 0. \tag{2.6b}$$

In the preceding

$$\alpha^2 = \omega^2/c_p^2 - \kappa^2, \quad \beta^2 = \omega^2/c_s^2 - \kappa^2 \tag{2.9}$$

where c_p and c_s are the dilatational (p) and shear (s) wave velocities. The first of the foregoing results describes an antisymmetric motion because the vector displacement field is antisymmetric upon reflection through the midplane $z = 0$. The second describes a symmetric displacement field.

Equations (2.6a,b) are the same as the classical frequency equations for straight-crest waves (plane strain) derived by Rayleigh in 1889 and analyzed by Lamb, giving frequency ω as an implicit transcendental function of κ, or vice versa. Equations (2.4)–(2.9) for real κ determine the mode shapes of free waves in an infinite plate, up to an arbitrary scale factor associated with each mode.

The behavior of the solution of equations (2.6) for complex as well as real values of κ has been extensively investigated [3]. For the present purposes, it will be sufficient to seek solutions for real wave numbers κ. Figure 2 shows the $\omega(\kappa)$ dependence as determined numerically for moderate and small values of real κ for the case of a glass plate of Poisson ratio, ν, equal to 0.21. Note that the dispersion relation is displayed by many branches on the $\omega - \kappa$ plane.

In the following, the branches will be ordered by numerals $m = 1,2,3,4, \ldots$, with odd integers for antisymmetric modes (dashed lines labeled by A_i in Fig. 2) and even integers for symmetric modes (solid lines labeled by S_i). They will also be referred to by their symmetry type and their order as given by the magnitude of their cutoff frequencies. Thus $m = 1$ is for the first antisymmetric branch A_1, and $m = 2$ for the first symmetric branch S_1, both starting at origin. The $m = 5$ designates the third antisymmetric branch, A_3, with κ ranging over real values from zero to infinity and ω/ω_s ranging from 3.0 to infinity, the $\omega_s\,(=\pi c_s/2h)$ being the frequency of the lowest thickness shear mode [3].

The concept of distinct branches is somewhat artificial in that the branches are continuosly connected from one to another by paths amongst complex values of κ. The existence of a multitude of branches indicates that at given κ, there are an infinite number of modes of wave propagation of the plate at different frequencies. At $\kappa = 0$, $\alpha = \omega/c_p$, and $\beta = \omega/c_s$ the wave normal is along the x-axis and the modes are called simple thickness modes [3].

Figures 3(a) and 3(b) show the radial group velocities $c_g = \partial\omega/\partial\kappa$ implied by the dispersion curves of Fig. 2. Note that the

Downloaded From: https://appliedmechanics.asmedigitalcollection.asme.org on 06/27/2019 Terms of Use: http://www.asme.org/about-asme/terms-of-use

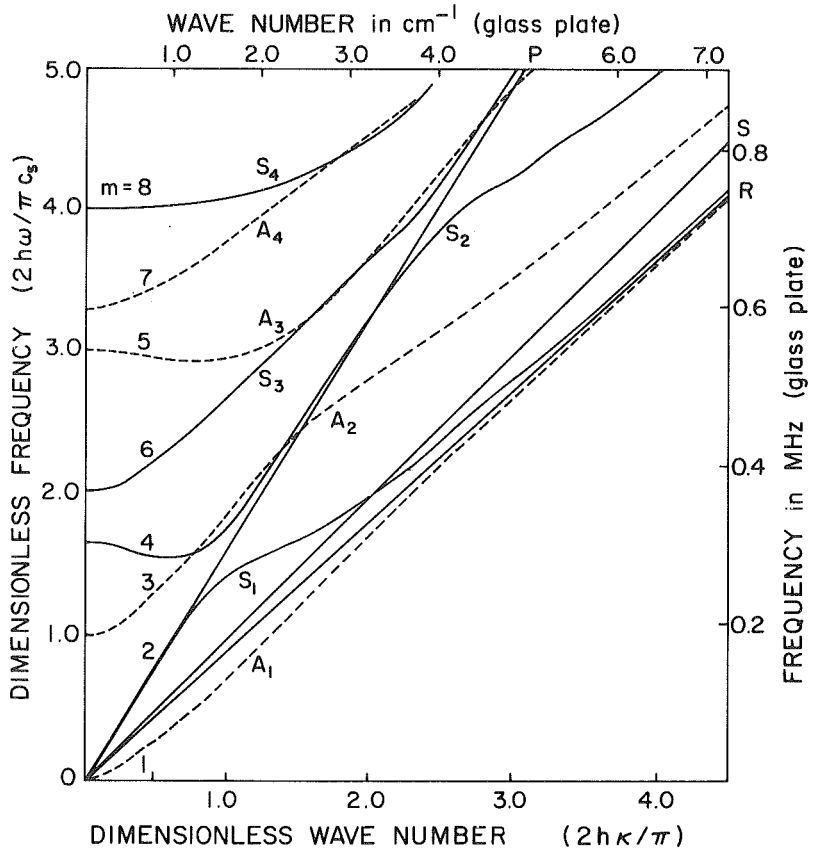

Fig. 2 First eight branches of dispersion relation for Rayleigh-Lamb waves in a plate ($\nu = 0.21$). (Glass plate: $2h = 0.960$ cm, $c_p = 0.576$ cm/μsec, $c_s = 0.349$ cm/μsec.) Erratum: the scale of the horizontal axis on the top should be doubled, and the wave number in cm^{-1} from 1.0 to 7.0 should be changed to 2.0 to 14.0.

Table 1 Maximum and minimum group velocities ($\nu = 0.21$) ($\omega_s = \pi c_s/2h$)

	Maxima		Minima	
Branch	c_g/c_s	ω/ω_s	c_g/c_s	ω/ω_s
A_1	0.99	0.93	–	–
A_2	1.17	1.80	0.68	3.01
A_3	0.14	3.04	0.71	5.73
	1.26	4.12		
A_4	0.79	4.22	0.77	4.69
S_1	1.59	0.00	0.49	1.55
S_2	0.21	1.61	0.70	4.38
	1.55	2.63		
S_3	0.97	2.95	0.93	3.53
	1.55	5.01	~0.6	~7.0

first symmetric branch (S_1 in Fig. 3(b) and first antisymmetric branch (A_1 in Fig. 3(a)) have asymptotic group velocities equal to the Rayleigh surface wave speed in a half space (slope of line OR in Fig. 2). Thus the modes lying on these branches at large κ are essentially Rayleigh surface waves. All other branches have asymptotic group velocities equal to the shear wave speed (slope of line OS in Fig. 2). At no point does any group velocity rise above the dilitational wave speed (slope of line OP in Fig. 2).

The maximum and minimum values of group velocities for each branch are listed in Table 1. In addition to the points indicated here, all branches have asymptotic stationary values of group velocity at infinite frequency, at, for S_1 and A_1, the Rayleigh wave speed $c_g/c_s = 0.9127$ and for other branches at the shear wave speed $c_g/c_s = 1.000$. The physical significance of these values will be discussed in Section 7.

3 Normal Modes of a Large Circular Plate

The expressions in equations (2.4) and (2.7) are the modes of free wave propagation in an infinite plate. When the plate is bounded by a cylindrical surface $r = R$, additional restrictions on the wave number κ will be imposed by the boundary conditions at $r = R$. The familiar boundary conditions of a traction-free surface ($\sigma_{rr} = \sigma_{rz} = 0$) or a rigid surface ($u_r = u_z = 0$), however, cannot be satisfied by these solutions [3, 19]. On the other hand, these solutions can be made to satisfy a rigid-smooth boundary condition, that is,

$$u_r = \sigma_{rz} = 0 \text{ at } r = R \tag{3.1}$$

The condition (3.1) can be shown to restrict κ to a set of discrete real irrational numbers,

$$\kappa = \kappa_n \equiv \gamma_n/R, \quad n = 1,2,\ldots \tag{3.2}$$

where γ_n are the roots of the radial frequency equation

$$J_0'(\gamma_n) = -J_1(\gamma_n) = 0. \tag{3.3}$$

For large n, the roots κ_n are nearly uniformly spaced and

$$\Delta\kappa = \kappa_{n+1} - \kappa_n \cong \pi/R \tag{3.4}$$

Hence, as we shall see later, the spacings of the roots are infinitesimally close when R approaches infinity.

From Fig. 2 we notice that for each value of $\kappa = \kappa_n$, there are an infinite number of values of ω, designated ω_{mn}. The

Downloaded From: https://appliedmechanics.asmedigitalcollection.asme.org on 06/27/2019 Terms of Use: http://www.asme.org/about-asme/terms-of-use

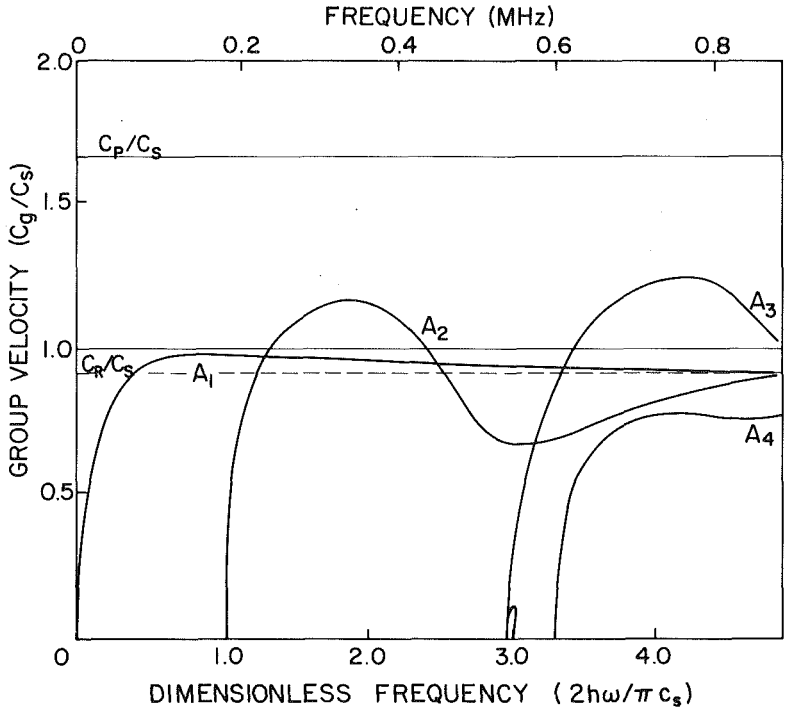

Fig. 3(*a*) Group velocity curves for antisymmetric branches

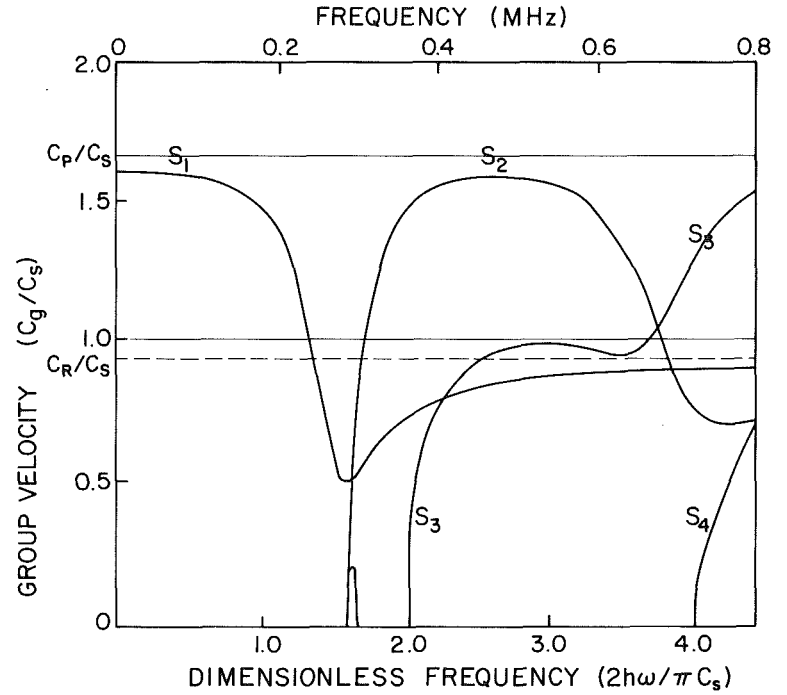

Fig. 3(*b*) Group velocity curves for symmetric branches

Fig. 3

index m corresponds to the order of branches and the ω_{mn} are the roots of Rayleigh-Lamb equation

$$R_{a,s}(\omega_{mn}, \kappa_n) = 0 \quad m, n = 1, 2, 3, \ldots \tag{3.5}$$

When α and β are calculated from equation (2.9) for each κ_n and ω_{mn}, the displacement vector of equation (2.4) represents a principal antisymmetric mode of vibration of a thick plate with finite radius R, and that of equation (2.7) a principal symmetric mode.

Since the two amplitudes B, C in equation (2.4) and A, D in equation (2.7) bear a constant ratio, we choose, according to equations (2.5) and (2.8)

$$B = 2\kappa^2\beta \sin \beta h$$

$$C = (\kappa^2 - \beta^2) \sin \alpha h \tag{3.6}$$

for the antisymmetric modes, and

$$A = -2\kappa^2\beta \cos \beta h$$

$$D = (\kappa^2 - \beta^2) \cos \alpha h \tag{3.7}$$

for the symmetric modes. When all κ's are appended with the subscript n, and all α's, β's, and ω's are appended with double subscripts mn, the principal modes are expressed by

$$\mathbf{u}_{mn}(\mathbf{x}) = U_{mn}(\mathbf{x})\hat{\mathbf{r}} + W_{mn}(\mathbf{x})\hat{\mathbf{z}} \tag{3.8}$$

In the foregoing, we have for antisymmetric modes (m = 1, 3, 5, . . .)

Downloaded From: https://appliedmechanics.asmedigitalcollection.asme.org on 06/27/2019 Terms of Use: http://www.asme.org/about-asme/terms-of-use

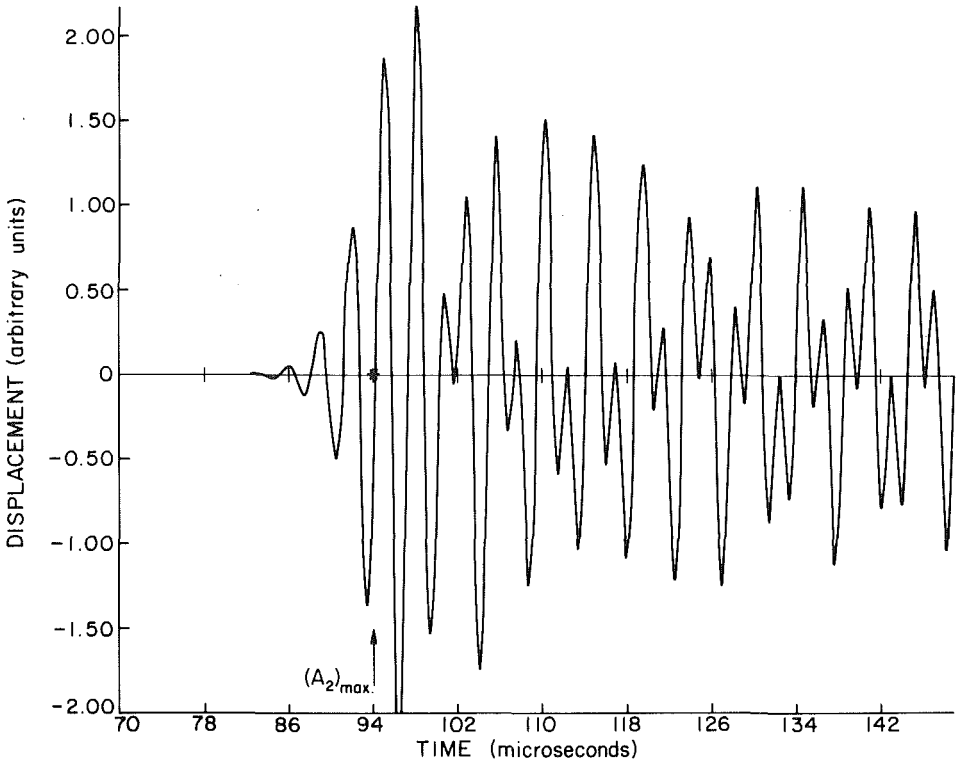

Fig. 4(*a*) The Airy phase of the second antisymmetric branch with the maximum group velocity $c_g = 1.17\, c_s$, $(A_2)_{max}$

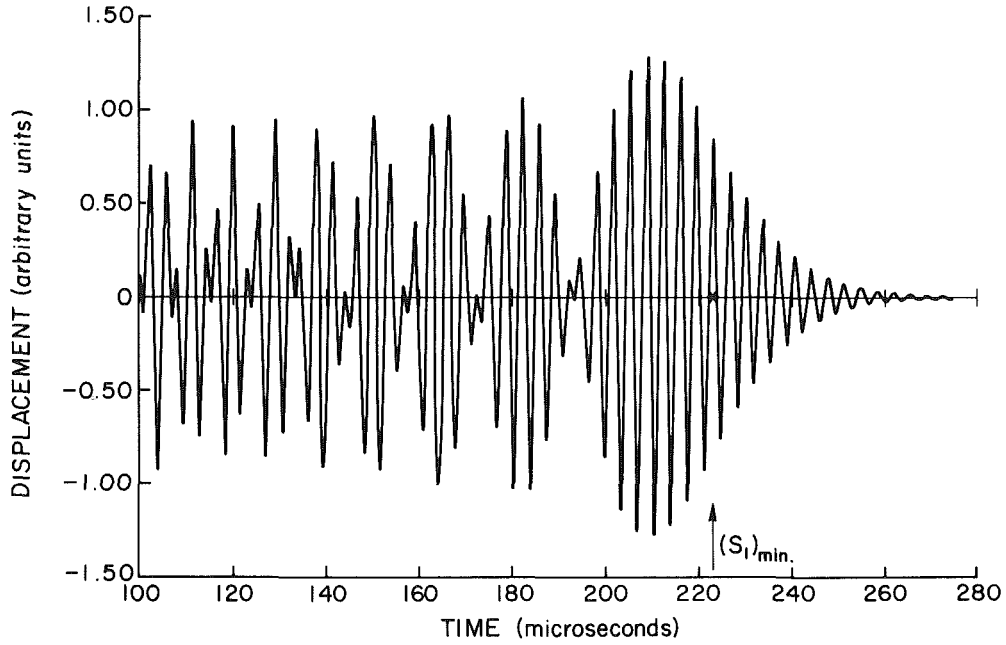

Fig. 4(*b*) The Airy phase of the first symmetric branch with the minimum group velocity $c_g = 0.49\, c_s$, $(S_1)_{min}$

Fig. 4 The Airy phase of the normal displacement at $r = 80\, h$.

$$U^a_{mn} = \beta_{mn}[2\kappa_n^2 \sin \beta_{mn}h \sin \alpha_{mn}z - (\kappa_n^2 - \beta_{mn}^2)\sin \alpha_{mn}h \sin \beta_{mn}z]\kappa_n J_0'(\kappa_n r)$$

$$W^a_{mn} = \kappa_n^2[2\alpha_{mn}\beta_{mn} \sin \beta_{mn}h \cos \alpha_{mn}z + (\kappa_n^2 - \beta_{mn}^2)\sin \alpha_{mn}h \cos \beta_{mn}z]J_0(\kappa_n r), \quad (3.9)$$

and for symmetric modes ($m = 2, 4, 6, \ldots$),

$$U^s_{mn} = \beta_{mn}[-2\kappa_n^2 \cos \beta_{mn}h \cos \alpha_{mn}z + (\kappa_n^2 - \beta_{mn}^2)\cos \alpha_{mn}h \cos \beta_{mn}z]\kappa_n J_0'(\kappa_n r)$$

$$W^s_{mn} = \kappa_n^2[2\alpha_{mn}\beta_{mn} \cos \beta_{mn}h \sin \alpha_{mn}z + (\kappa_n^2 - \beta_{mn}^2)\cos \alpha_{mn}h \sin \beta_{mn}z]J_0(\kappa_n r), \quad (3.10)$$

As in equation (2.9), α and β are determined by

$$\alpha_{mn}^2 = \omega_{mn}^2/c_p^2 - \kappa_n^2$$

$$\beta_{mn}^2 = \omega_{mn}^2/c_s^2 - \kappa_n^2. \quad (3.11)$$

When properly normalized by a constant, $\mathbf{u}_{mn}(\mathbf{x})$ are also called the *normal modes* of the vibrating plate.

Restoring the time factor $\exp(-i\omega t)$ and superposing all

Downloaded From: https://appliedmechanics.asmedigitalcollection.asme.org on 06/27/2019 Terms of Use: http://www.asme.org/about-asme/terms-of-use

normal modes, we can express the general motion of the freely vibrating plate,

$$\mathbf{u}(\mathbf{x}, t) = \sum_{m=1}^{\infty} \sum_{n=1}^{\infty} A_{mn}[U_{mn}(\mathbf{x})\hat{\mathbf{r}} + W_{mn}(\mathbf{x})\hat{\mathbf{z}}]e^{-i\omega_{mn}t} \quad (3.12)$$

The circular plate is free of stresses on the two flat surfaces (equation 2.2) and is rigidly and smoothly constrained at the circumference (equation 3.1). The complex coefficients, A_{mn}, are to be determined from the hitherto unspecified initial conditions.

4 Forced Vibration of a Large Circular Plate

In this section, we present the formal solution of the motion of a finite plate under the excitation of a time-dependent body force $\mathbf{F}(\mathbf{x}, t)$. The motion is governed by equation (2.1) with boundary conditions (2.2) and (3.1), and initial conditions (2.3). The solution is a special case of a general class of solutions for elastodynamic equations derived by the method of eigenfunction expansions [13–15]. We summarize this method in the following subsection and present the solution for the circular plate in the next one.

4.1 Method of Eigenfunction Expansion. A linear differential operator $\mathbf{L}$ is self-adjoint in a vector space S of vector functions defined in a volume Ω with respect to the inner product

$$(\mathbf{u}, \mathbf{v}) = \int_{\Omega} \mathbf{u} \cdot \mathbf{v} dV \quad (4.1)$$

if for all $\mathbf{u}$ and $\mathbf{v}$ in S

$$\int_{\Omega} \mathbf{v} \cdot \mathbf{L}(\mathbf{u}) dV = \int_{\Omega} \mathbf{u} \cdot \mathbf{L}(\mathbf{v}) dV \quad (4.2)$$

Restricting the space S to suitably continuous functions that satisfy homogeneous boundary conditions on the boundary of Ω, one finds that the operator $\mathbf{L}$ defined by equation (2.1) is self-adjoint (and so is its generalization to anisotropic and inhomogeneous media) for the following boundary conditions:

At each point of the boundary, let $\hat{\mathbf{e}}_i$ be three mutually perpendicular directions. The self-adjoint boundary conditions are

$$\hat{\mathbf{e}}_i \cdot [a_i \mathbf{u} + b_i \mathbf{T}] = 0, \quad (i = 1, 2, 3) \quad (4.3a)$$

$\mathbf{T}$ being the surface traction on the boundary associated with the field $\mathbf{u}$. The a_i and b_i may take any values as long as they are not both zero at the same point of the boundary. Traction-free boundary conditions, for example, may be represented by $a_i = 0$, $b_i = 1$ for all i. Rigid-smooth boundary conditions may be represented by $a_i = 1$, $b_i = 0$ for the rigid normal direction $\hat{\mathbf{e}}_i = \mathbf{n}$, and by $a_j = 0$, $b_j = 1$ for the smoothly sliding directions $\hat{\mathbf{e}}_j$ = tangent directions. We may express these boundary conditions symbolically as

$$\mathbf{B}(\mathbf{u}, \mathbf{T}) = 0 \quad \text{on boundary.} \quad (4.3b)$$

Let $\mathbf{u} = \mathbf{u}^{(m)}(\mathbf{x}) \exp(-i\omega_m t)$ be the solution of equation (2.1) without the body force $\mathbf{F}$, satisfying the boundary conditions (4.3), that is,

$$\mathbf{L}(\mathbf{u}^{(m)}) = -\rho\omega_m^2 \mathbf{u}^{(m)} \text{ in } \Omega \quad (4.4)$$

and

$$\mathbf{B}(\mathbf{u}^{(m)}, \mathbf{T}^{(m)}) = 0 \text{ on boundary} \quad (4.5)$$

The $\mathbf{u}^{(m)}$ are then the eigenfunctions of the operator $\mathbf{L}$, and ω_m the eigenvalues. For self-adjoint boundary conditions, the eigenfunctions form an orthogonal set with the weighting function ρ.

$$\int_{\Omega} \rho \mathbf{u}^{(m)} \cdot \mathbf{u}^{(n)} dV = 0 \quad m \neq n \quad (4.6)$$

and all eigenvalues ω_m^2 can be shown to be real and non-negative [13]. The norm of the eigenfunctions is given by

$$M^{(m)} = \int_{\Omega} \rho \mathbf{u}^{(m)} \cdot \mathbf{u}^{(m)} dV \quad (4.7)$$

Since the eigenfunctions form a complete set [14], any arbitrary functions in the space S can be expanded in a series of these orthogonal eigenfunctions. This enables one to solve the inhomogeneous equation (2.1) when $\mathbf{F} \neq 0$. Let

$$\mathbf{u}(\mathbf{x}, t) = \sum_{m} \mathbf{u}^{(m)}(\mathbf{x}) q_m(t) \quad (4.8)$$

where $q_m(t)$ are time-dependent coefficients. Substituting the series into equation (2.1), multiplying (inner product) by $\mathbf{u}^{(n)}(x)$, integrating the product over the entire volume Ω, and invoking the orthogonality conditions (4.6), we find

$$M^{(m)}\left[\frac{d^2 q_m^{(t)}}{dt^2} + \omega_m^2(t) q_m(t)\right] = F^{(m)}(t) \quad (4.9)$$

where

$$F^{(m)}(t) = \int_{\Omega} \mathbf{u}^{(m)}(\mathbf{x}) \cdot \mathbf{F}(\mathbf{x}, t) dV \quad (4.10)$$

With quiescent initial conditions equation (2.3), we set

$$q_m(0) = \dot{q}_m(0) = 0. \quad (4.11)$$

The general solution of equation (4.9) is then

$$q_m(t) = \frac{1}{\omega_m M^{(m)}} \int_0^t F^{(m)}(\tau) \sin \omega_m (t - \tau) d\tau \quad (4.12)$$

Substitution of the foregoing into equation (4.8) completes the solution of equation (2.1) with boundary conditions (4.3), and initial conditions (2.3).

4.2 Transient Motion of a Circular Plate. The normal modes given in equations (3.8)–(3.10) are for a circular plate bounded by $z = \pm h$ and $r = R$. The boundary conditions are specified by equation (2.2) and equation (3.1). It has already been demonstrated that traction-free and rigid-smooth boundary conditions are self-adjoint. Thus, the boundary conditions for the present circular plate are self-adjoint. According to equations (4.6) and (4.7) the normal modes $\mathbf{u}_{mn}(\mathbf{x})$ of equation (4.8) are orthogonal,

$$2\pi \int_{-h}^{h} \int_0^R [\rho \mathbf{u}_{mn}(\mathbf{x}) \cdot \mathbf{u}_{pq}(\mathbf{x})] r dr dz = \delta_{mp} \delta_{nq} M^{(mn)} \quad (4.13)$$

where δ_{mn} is the Kronecker delta.

The transient motion of the plate that is quiescent at $t = 0$ is derived from equations (4.8), (4.10), (4.12),

$$\mathbf{u}(r, z, t) = \sum_{m=1}^{\infty} \sum_{n=1}^{\infty} \frac{1}{M^{(mn)}} \mathbf{u}_{mn}(r, z) Q^{(mn)}(t) \quad (4.14)$$

where

$$Q^{(mn)}(t) = \frac{1}{\omega_{mn}} \int_0^t F^{(mn)}(\tau) \sin \omega_{mn}(t - \tau) d\tau \quad (4.15)$$

and

$$F^{(mn)}(t) = 2\pi \int_{-h}^{h} \int_0^R \mathbf{F}(r, z, t) \cdot \mathbf{u}_{mn}(r, z) r dr dz \quad (4.16)$$

The body force $\mathbf{F}(r, z, t)$ has not yet been specified but for the present problem it must be axially symmetric; the normal modes $\mathbf{u}_{mn}(r, z)$ are given by equation (3.9) when $m = 1, 3, 5 \ldots$, and by equation (3.10) when $m = 2, 4, 6 \ldots$.

The normalization constant $M^{(mn)}$ can be analytically evaluated in this case,

$$M^{(mn)} = 2\pi \int_{-h}^{h} \int_0^R [\rho \mathbf{u}_{mn}(r, z) \cdot \mathbf{u}_{mn}(r, z)] r dr dz \quad (4.17)$$

The part that depends on r can be evaluated by applying the integral formula [formula 11.4.2, reference 20]

Downloaded From: https://appliedmechanics.asmedigitalcollection.asme.org on 06/27/2019 Terms of Use: http://www.asme.org/about-asme/terms-of-use

$$\int_0^R J_\nu^2(\kappa_n r)\,rdr = \frac{1}{2}R^2\begin{cases}(J_0(\kappa_n R))^2 & \nu=0\\ (J_1'(\kappa_n R))^2 & \nu=1\end{cases} \tag{4.18}$$

where $\kappa_n R$ are the roots of $J_0'(\kappa R) = -J_1(\kappa R) = 0$. The z-dependent parts are common integrals. The final results are presented in the following, for sufficiently large R that $(J_0(\kappa_n R))^2 \approx (J_1'(\kappa_n R))^2 \approx 2/(\pi\kappa_n R)$ and for $M_\infty^{(mn)}$ defined by

$$M^{(mn)} = RM_\infty^{(mn)}. \tag{4.19}$$

For m odd (antisymmetric modes)

$$M_\infty^{(mn)} = \frac{2\rho}{\kappa}[B^2(\omega^2 h/c_p^2 + (\alpha^2-\kappa^2)\sin 2\alpha h/2\alpha) + C^2\kappa^2(\omega^2 h/c_s^2 - (\beta^2-\kappa^2)\sin 2\beta h/2\beta) + 4BC\kappa^2 \sin\alpha h \cos\beta h] \tag{4.20a}$$

and for m even (symmetric modes)

$$M_\infty^{(mn)} = \frac{2\rho}{\kappa}[A^2(\omega^2 h/c_p^2 - (\alpha^2-\kappa^2)\sin 2\alpha h/2\alpha) + D^2\kappa^2(\omega^2 h/c_s^2 + (\beta^2-\kappa^2)\sin 2\beta h/2\beta) + 4AD\kappa^2 \cos\alpha h \sin\beta h]. \tag{4.20b}$$

In the foregoing, κ must be understood as having index n and A, B, C, D, α and β as having indices m and n. A, B, C, and D are defined in equations (3.6) and (3.7).

5 Transient Waves in an Infinite Plate

We return to the original problem as posed in Section 2 of an infinite plate excited by a body force $\mathbf{F}(\mathbf{x}, t)$. The solution can be constructed directly from that of a finite plate, as given in the preceding section by letting the radius R approach infinity. Physically, this means that we are ignoring the reflection of waves from the edge at $r = R$, or considering only the time span before the waves generated by the source reach the reflecting edge. Hence, it is immaterial what type of boundary conditions are imposed at the edge.

For some applications one need not take the limit $R \to \infty$, as long as R is large enough that reflections from the outer boundary do not arrive within the times of interest. If R is taken merely large, but not infinite, one is left with a sum over discrete modes instead of the integral, equation (5.1). The integral is a more convenient form for numerical and analytic study, as one need not solve the transcendental equation (3.3) and because one may employ FFT techniques for its evaluation. The integral form is also more generally applicable to very late times or very large distances, without the restrictions $r < R$, $t < (2R-r)/c_p$. Nevertheless, as the numerical evaluation of integrals is always an approximation, the sum form, with $R \neq \infty$, may be more accurate for numerical work.

5.1 General Solutions. As R approaches infinity, the normalization constant $M^{(mn)}$ that contains a factor R^{-1} becomes infinitesimal. Thus each mode in the sum of equation (4.14) contributes an infinitesimal amount to the total amplitude. But in the same limit, the number of modes indexed by n for each value of m is increasing because the spacing between two successive roots, $\Delta\kappa \cong \pi/R$ in equation (3.4), approaches zero. Therefore, in the limit as $R \to \infty$, the summation over the index n of equation (4.14) is replaced by an integration over the continuous wave number κ. The integration is carried out for each branch, indexed by m, from $\kappa = 0$ to $\kappa = \infty$.

Replacing first $1/M^{(mn)}$ in equation (4.14) by $\Delta\kappa/\pi M_\infty^{(mn)}$, taking the limit $\Delta\kappa \to 0$ while $R \to \infty$, and then dropping all subscripts n, we obtain

$$\mathbf{u}(r, z, t) = \sum_{m=1}^{\infty}\int_0^\infty \frac{\mathbf{u}_m(r, z; \kappa)}{\pi M_\infty^{(m)}(\kappa)} Q^{(m)}(t; \kappa)\,d\kappa \tag{5.1}$$

where

$$Q^{(m)}(t; \kappa) = \frac{1}{\omega_m(\kappa)}\int_0^t F^{(m)}(\tau;\kappa)\sin[\omega_m(\kappa)(t-\tau)]d\tau \tag{5.2}$$

$$F^{(m)}(t; \kappa) = 2\pi\int_{-h}^{h}\int_0^\infty \mathbf{F}(r, z, t)\cdot\mathbf{u}_m(r, z; \kappa)\,rdrdz \tag{5.3}$$

Note that the normal modes $\mathbf{u}_m(r, z; \kappa)$ in the foregoing are the same as those given in equations (3.6)–(3.10) except that the discrete wave numbers κ_n are replaced by a continuous variable κ. For each value of κ, there is still a discrete set of values for ω, and hence also for α and β, each indexed by the subscript m. On the other hand, for each m, ω varies continuously with κ as governed by the Rayleigh-Lamb equations (2.6)

$$R_a(\omega_m, \kappa) = 0 \qquad m = 1, 3, 5, \ldots$$

$$R_s(\omega_m, \kappa) = 0 \qquad m = 2, 4, 6, \ldots \tag{5.4}$$

In the final expressions (5.1)–(5.3), $\mathbf{u}_m(r, z; \kappa)/M_\infty^{(m)}(\kappa)$, where $M_\infty^{(m)}(\kappa)$ is given by equation (4.20), represents the spatial variation of the mode indexed by the branch number, m, and the radial wave number κ. $F^{(m)}(t, \kappa)$ represents the generalized time-dependent force acting on the mode (m, κ), and $Q^{(m)}(t, \kappa)$ is the time-dependent response of the amplitude of the mode. The total plate response in (5.1) is represented as a superposition of the response of each normal mode. The choice of receiver location and the choice of loading here find their expression through the "receiver function" $\mathbf{u}_m$ and through the "source function" Q.

It is particularly revealing to note that the modal factor depends on the source character and location via the integral of $F^{(m)}$ in equation (5.3). Thus if the force $\mathbf{F}(r, z, t)$ is orthogonal to a mode $\mathbf{u}^{(m)}(r, z, \kappa)$, or more simply, if the simple point force acts at a node of the mode in question, that mode is not excited by the force; analogously, a string plucked at its midpoint is not excited into any even harmonics.

5.2 Waves Generated by a Stationary Concentrated Force. For the remaining part of this paper, we consider a vertical, stationary, concentrated force at $(0, 0, z_0)$, the time dependence being a Heaviside step function. We thus express $\mathbf{F}(\mathbf{x}, t)$ as

$$\mathbf{F}(\mathbf{x}, t) = Q_0\frac{\delta(r)}{2\pi r}\delta(z-z_0)H(t)\,\hat{\mathbf{z}} \tag{5.5}$$

where Q_0 is the magnitude of the applied force. Substituting it into equation (5.3), we find

$$F^{(m)}(t, \kappa) = H(t)f_m(z_0, \kappa) \tag{5.6}$$

where, for antisymmetric modes,

$$f_m(z_0, \kappa) = Q_0\kappa^2[2\alpha_m\beta_m \sin\beta_m h \cos\alpha_m z_0 + (\kappa^2-\beta_m^2)\sin\alpha_m h \cos\beta_m z_0] \quad m = 1, 3, 5, \ldots \tag{5.7a}$$

and for symmetric modes,

$$f_m(z_0, \kappa) = Q_0\kappa^2[2\alpha_m\beta_m \cos\beta_m h \sin\alpha_m z_0 + (\kappa^2-\beta_m^2)\cos\alpha_m h \sin\beta_m z_0] \quad m = 2, 4, 6, \ldots, \tag{5.7b}$$

The time function in equation (5.2) can then easily be integrated,

$$Q^{(m)}(t, \kappa) = f_m(z_0, \kappa)\frac{1}{\omega_m^2(\kappa)}[1-\cos\omega(\kappa)t]H(t) \tag{5.8}$$

To summarize, the final result for transient waves in an infinite plate with thickness $2h$, which is excited by a concentrated vertical force being placed suddenly at $t = 0$, $r = 0$, and $z = z_0$ is

Downloaded From: https://appliedmechanics.asmedigitalcollection.asme.org on 06/27/2019 Terms of Use: http://www.asme.org/about-asme/terms-of-use

$$\mathbf{u}(r, z, t) =$$

$$H(t) \sum_{m=1}^{\infty} \int_0^{\infty} f_m(z_0, \kappa) \frac{\mathbf{u}_m(r, z; \kappa)}{\pi M_m(\kappa)} \left[\frac{1 - \cos \omega_m(\kappa) t}{\omega_m^2(\kappa)} \right] d\kappa. \quad (5.9)$$

In the foregoing, the $f_m(\kappa)$ are given in equation (5.7), and the modes for the mth branch are

$$\mathbf{u}_m(r, z; \kappa) = U_m(r, z; \kappa)\hat{\mathbf{r}} + W_m(r, z; \kappa)\hat{\mathbf{z}} \quad (5.10)$$

where the U_m and W_m functions are given in equations (3.9) and (3.10). The $M_m(\kappa)$ equal $M_\infty^{(m)}$ in equation (5.1) and are given by equation (4.20). The ω_m are related to κ by equation (5.4). These equations form the basis for the stationary phase analysis and for the numerical evaluations.

6 Transient Response by Integral Transforms

The standard procedure for the analysis of the axisymmetric response of a plate to dynamic loadings entails the performance of two integral transforms on the equations of motion, one on the time variable, the other on a spatial variable. This procedure is thoroughly discussed by Miklowitz (Chapter 7, reference [4]) for a line load and plane strain. We will not present the analogous procedure for the axisymmetric case but will describe it and then compare it with the method of eigenfunction expansion.

For the double transform technique equation (2.1) is re-expressed as decoupled scalar equations for the displacement potentials ϕ and ψ involving the force potentials f and g, where

$$\mathbf{u} = \nabla\phi + \nabla \times \nabla \times (\psi\hat{\mathbf{z}}) \quad (6.1)$$

$$\mathbf{F} = \nabla f + \nabla \times \nabla \times (g\hat{\mathbf{z}}). \quad (6.2)$$

Similarly equations (2.2) are rewritten as coupled boundary conditions on ϕ and ψ. A Fourier (or Laplace) transform in time and a Hankel transform in radial position r are performed on these rewritten equations. The resulting coupled inhomogeneous ordinary differential equations for the double transforms of ϕ and ψ may be solved and the inverse double transforms performed to obtain the actual displacement potentials. $\mathbf{u}$ is then constructed from (6.1).

If the inverse Fourier transform is performed before the inverse Hankel transform and evaluated by means of contour integration and the theory of residues, the resulting expression for $\mathbf{u}$ resembles (5.9), and must necessarily be identical to equation (5.9). Alternatively, one may do the inverse Hankel transform first, also by residues, and directly obtain the spectrum of the response. The transient solution would then be obtained by numerical inverse Fourier transformation.

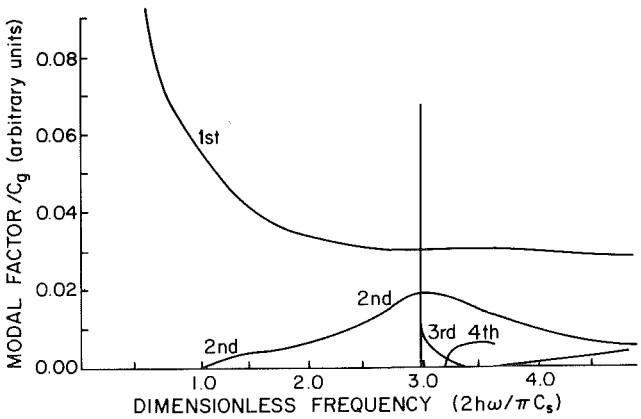

Fig. 5(a) Antisymmetric modes

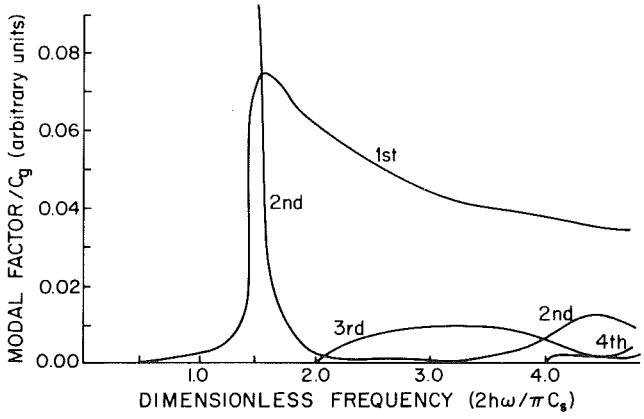

Fig. 5(b) Symmetric modes

Fig. 5 Modal factor/group velocity

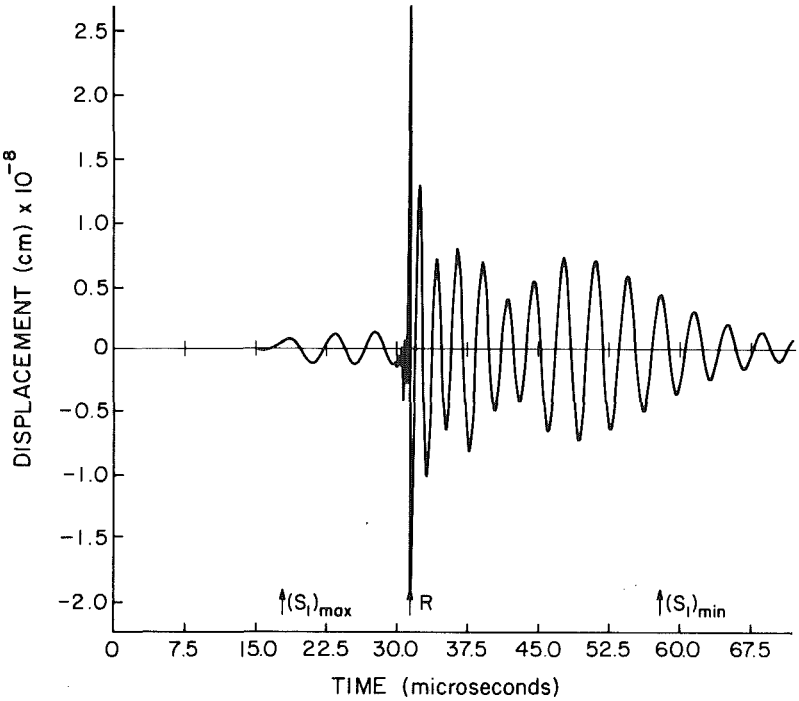

Fig. 6(a) First symmetric branch (S_1)

Downloaded From: https://appliedmechanics.asmedigitalcollection.asme.org on 06/27/2019 Terms of Use: http://www.asme.org/about-asme/terms-of-use

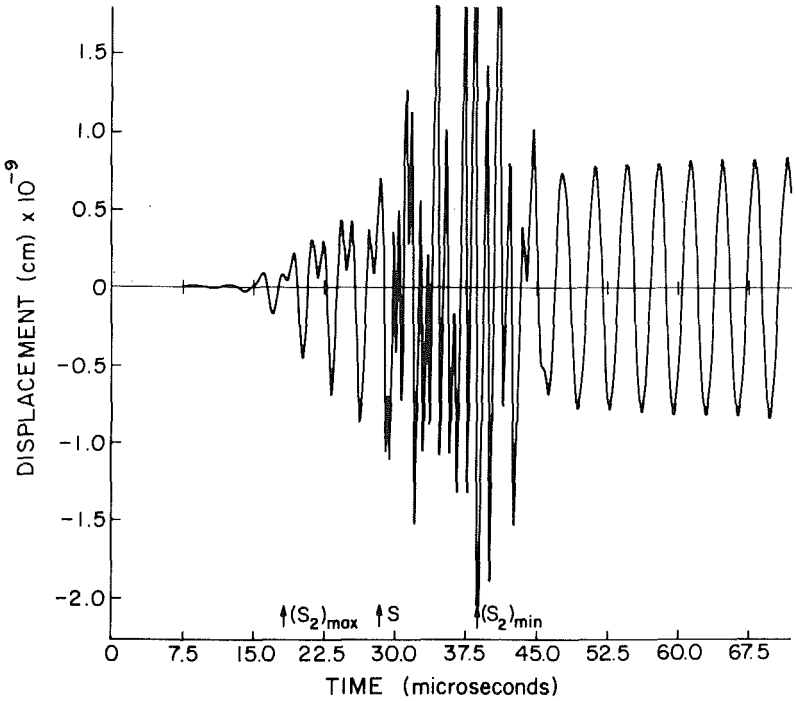

Fig. 6(*b*) Second symmetric branch (S_2)

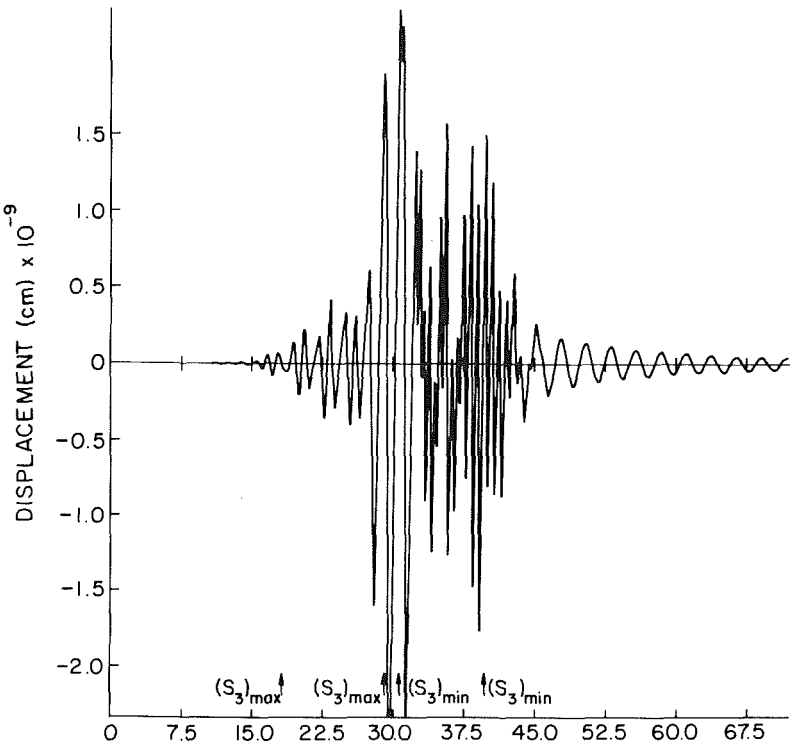

Fig. 6(c) Third symmetric branch (S_3)

Fig. 6 Normal displacement due to individual symmetric branches ($r = 10$ cm)

One can with reason claim that the method of integral transforms is more versatile in that with it one has two options of evaluating the inverse transforms. One option leads directly to the solution by the method of normal modes, and the other yields the same transient solution as well as the spectrum of the transient response. The practical value of this aspect of the double transform method is, however, limited, because evaluation of the spectrum requires the location of all complex roots of the Rayleigh-Lamb function as well as the real roots. Furthermore, for buried forces the method of integral transforms requires the decomposition of the force into force potentials f and g which is tedious, if not very difficult especially in the case of nonaxisymmetric loads. The method then requires the solutions of the ordinary differential equations in z. These solutions are very complex in the general case of buried distributed forces. Miklowitz's applications of the integral transform method have been confined to those loads representable by inhomogeneous boundary conditions

Downloaded From: https://appliedmechanics.asmedigitalcollection.asme.org on 06/27/2019 Terms of Use: http://www.asme.org/about-asme/terms-of-use

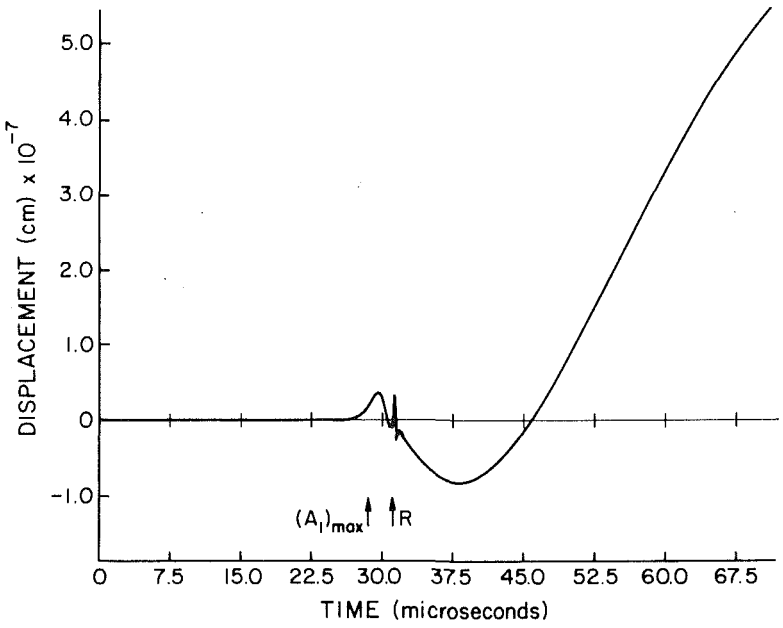

Fig. 7(*a*) First antisymmetric branch (A_1)

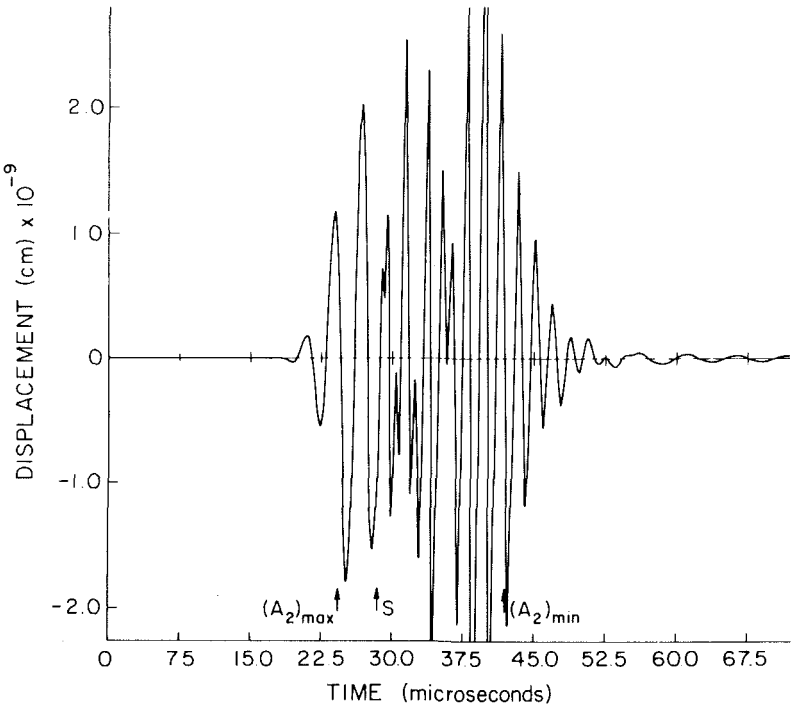

Fig. 7(*b*) Second antisymmetric branch (A_2)

Fig. 7 Normal displacement due to individual antisymmetric branches (r = 10 cm)

such as vertical surface forces where the procedure is much simplified.

It is our contention that the integral transform method is analytically the more cumbersome and, for many applications, the less versatile. It can further be criticized on the grounds that the use of the abstract quantities, the transforms of the displacement potentials, obscures the simple physics which is revealed in the method of explicit expansion in normal modes.

7 Analysis by the Method of Stationary Phase

Analysis of integrals such as equation (5.9) has in the past been confined essentially to far field asymptotic approximations based on the method of stationary phase. One recognizes that at large r, ($r >> h$ or $t >> h/c_p$) the variation of the integrand with κ is dominated by the rapid oscillations of the Bessel functions $J_0(\kappa r)$ and $J_0'(\kappa r)$ in $\mathbf{u}_m$ and the function cos $\omega_m(\kappa)t$. But if $\kappa = \kappa_0$ is such that $|\partial\omega/\partial\kappa|_{\kappa=\kappa_0} = r/t$ then the oscillations of the cosine function and the Bessel functions are in phase, whereupon in the vicinity of κ_0 the integrand is, for a short range in κ, not rapidly oscillating. The displacement time trace at r is thus dominated by a sum of terms oscillating in time; each of them represents a simple harmonic wave train at a frequency such that $|\partial\omega/\partial\kappa| = r/t$. This is the basis for the well-known "group velocity analysis" [22] or "period-time of occurrence relations" [4]. The relative strengths of these many contributions depends of course on the magnitudes of

Downloaded From: https://appliedmechanics.asmedigitalcollection.asme.org on 06/27/2019 Terms of Use: http://www.asme.org/about-asme/terms-of-use

$f_m(\kappa)/M_m(\kappa)$ when evaluated at $\kappa = \kappa_0$. This analysis shows further that each such contribution is inversely proportional to $(t|\partial^2\omega/\partial\kappa^2|)^{1/2}$ and thus the points at which the group velocity is nearly stationary are expected to be the most important. The actual point where $\partial^2\omega/\partial\kappa^2 = 0$ in fact contributes an amount proportional to $(t\partial^3\omega/\partial\kappa^3)^{-1/3}$ and thus dominates at sufficiently large t [23]. The contributions from such points are called the "Airy phases."

As an illustration, we consider the normal displacement u_z at r and $z = +h$, the force Q_0 of equation (5.5) being applied at the surface of the plate ($z_0 = +h$),

$$u_z(r, h, t) = H(t) \sum_{m=1}^{\infty} \int_0^{\infty} f_m(h, \kappa) \frac{W_m(r, h; \kappa)}{\pi M_m(\kappa)} \frac{1 - \cos \omega_m(\kappa) t}{\omega_{m(\kappa)}^2} d\kappa \qquad (7.1)$$

We separate out the r-dependence of W_m of equation (5.10), or equations (3.9) and (3.10), and rewrite the previous result as

$$u_z(r, h, t) = H(t) \sum_{m=1}^{\infty} u_{zm}(r, h, t)/\pi \qquad (7.2)$$

where

$$u_{zm}(r, h, t) = \int_0^{\infty} Z_m(h, \kappa) J_0(\kappa r)(1 - \cos \omega_m t)\, d\kappa \qquad (7.3)$$

and

$$Z_m(h, \kappa) = f_m(h, \kappa) W_m(r, h; \kappa)/[M_m(\kappa)\omega_m^2(\kappa) J_0(\kappa r)]$$

The integration may be separated into two parts. The time-independent part yields the "statical deflection" for each branch corresponding to the long-time contribution of the step loading. The time-dependent part can be evaluated by the method of stationary phase, by noting that for large t and r,

$$J_0(\kappa r)\cos \omega_m t \sim (2\pi\kappa r)^{-1/2} Re[e^{i(\kappa r - \omega_m t - \pi/4)} + e^{i(\kappa r + \omega_m t - \pi/4)}] \qquad (7.4)$$

Along each branch of the group velocity curves (Fig. 3), there might be more than one maximum and minimum point. Corresponding to each stationary point, there are a set of values for the wave number, frequency, and group velocity, which are designated as κ_0, ω_0, c_{g0} respectively, where

$$c_{g0} = (\partial\omega/\partial\kappa)_{\kappa=\kappa_0} \qquad (7.5)$$

Since the arrival time of this wave-train group at r is $t_0 = r/c_{g0}$, the group with the maximum speed will be well separated from the group with the minimum speed on the time trace recorded at r. For time t around t_0, the dominant value of the time-dependent part of the integral, equation (7.3), is, [22] the contribution from the modes near the stationary point in the group velocity curve, the "Airy phase."

$$u_{zm} \sim (2\pi\kappa_0 r)^{-1/2} Z_m(h, \kappa_0)(t\omega_0'')^{-1/3} \mathrm{Ai}(\tau)\cos(\omega_0 t - \kappa_0 r + \pi/4) \qquad (7.6)$$

where

$$\tau \equiv c_{g0}(t - t_0)(t\omega_0''/2)^{-1/3} \qquad (7.7)$$

In the foregoing, $\omega_0'' = (d^3\omega/d\kappa^3)_{\kappa=\kappa_0}$ and Ai is the Airy function. The preceding time trace may be described as a rapidly varying sinusoidal function of time with a slowly varying envelope of an Airy function. The strength of this contribution to the total displacement depends of course on the magnitude of the function $Z_m(\kappa)$ at the point κ_0.

Typical plots of the foregoing expression are given in Figs. 4 where the factor $Z/(2\pi\kappa_0 r)^{1/2}$ has been replaced by unity and where the plate parameters have been chosen, $\nu = 0.21$, $2h = 0.960$ cm, and $c_s = 0.349$ cm/μsec. The receiver is located a distance of 40 thicknesses from the source. Figure 4(a) shows the case $\omega_0'' < 0$, i.e., the case of a maximum group velocity for the second antisymmetric branch at $\omega_0 = 1.805\ \omega_s$ ($\omega_s = \pi c_s/2h$), $\kappa_0 = 0.94\ (\pi/2h)$, $c_{g0} = 1.17\ c_s$ and $\omega_0'' = -1.34\ (2h/\pi)^2\ c_s$. Figure 4($b$) shows the case of the minimum group velocity for the first symmetric branch at $\omega_0 = 1.55\ \omega_s$, $\kappa_0 = 1.24\ (\pi/2h)$, $c_{g0} = 0.49\ c_s$, and $\omega_0'' = 3.37\ (2h/\pi)^2\ c_s$. The former case may be called a "mode arrival," the latter a "mode disappearance." As shown in the foregoing one might expect curves of these forms to dominate the time traces for sufficiently large source-receiver separations. Wave packets with these shapes will be found in the general results shown in the next section.

Stationary phase analysis of integrals such as the preceding has been employed at least since the time of Kelvin (1887) and indeed is the only analysis possible in the far field short of extensive numerical work. Practical difficulties exist with it however, chiefly describable by the following unanswered questions: How large must r and t be in order that the Airy phases are the major contributions? What are the appropriate expressions, different from equation (7.6), at those maxima and minima that exist at the end points, $\kappa = 0$ or $\kappa = \infty$? Furthermore there exist points where $\omega'' \approx \omega''' \approx 0$ where expression (7.6) is again invalid. There also exist points where $\omega'' = 0$ and $Z_m \approx 0$, where again the preceding expression is invalid.

For convenience, we call $Z_m(h, \kappa)$ of equation (7.3) the "modal factor." It depends on the loading function, $\omega_m^{-2} f_m(h, \kappa)$, as well as the normal mode, $U_m(r, h; \kappa)/J_0(\kappa r)$. It may become zero or infinite at certain values of κ, a point not considered in the usual problems of stationary phase analyses. In Fig. 5 we show $Z_m(h)$ (divided by $|c_g| = |d\omega/d\kappa|$) as a function of ω/ω_s for the first four branches of antisymmetric modes (Fig. 5(a)), and first four symmetric branches (Fig. 5(b)). These curves are dependent on the vertical location of the source ($z_0 = h$) and receiver ($z = h$), the time function of the concentrated force (a step time function), but independent of the radial distance r and time t. It is interesting to note that values of the modal factor are zero, or nearly zero, at the maxima of group velocities of many branches (Fig. 3). These modes are thus much less significant then otherwise have been expected.

The conceptual complexities required of a thorough pursuit of this method are many. Thus in the light of its approximate nature, we suggest that its value is chiefly for qualitative analysis, and in the initial interpretation of measured plate responses. This qualitative theory may be compared to the numerical results of the exact integral as given in the next section.

8 Surface Response of a Plate Due to a Concentrated Force

The integrals in equations (7.2) and (7.3) for the vertical displacement component, u_z, have been evaluated by a numerical integration. The algorithm employed for the numerical integration entailed a conversion of independent variable from κ to ω and then an integration by Fast Fourier Transform techniques (FFT). Because the conversion of independent variable introduces an inverse factor of group velocity to the integrand and because FFT techniques do not allow for varying step sizes in the integration, the low group velocity ranges are not accurately computed by this technique. Integration for these ranges was done directly in the wave number domain with a trapazoidal rule. This algorithm was thought to be the most efficient and accurate for a not too large range in source-receiver distances. At very large distances where the integrand is in general a rapidly varying function of κ (or ω), the integral would probably be most efficiently and accurately evaluated by a method appropriate to the numerical integration of rapidly and sinusoidally varying functions [24]. The computing costs varied with the source-receiver distance but averaged about 1 dollar per integration.

Downloaded From: https://appliedmechanics.asmedigitalcollection.asme.org on 06/27/2019 Terms of Use: http://www.asme.org/about-asme/terms-of-use

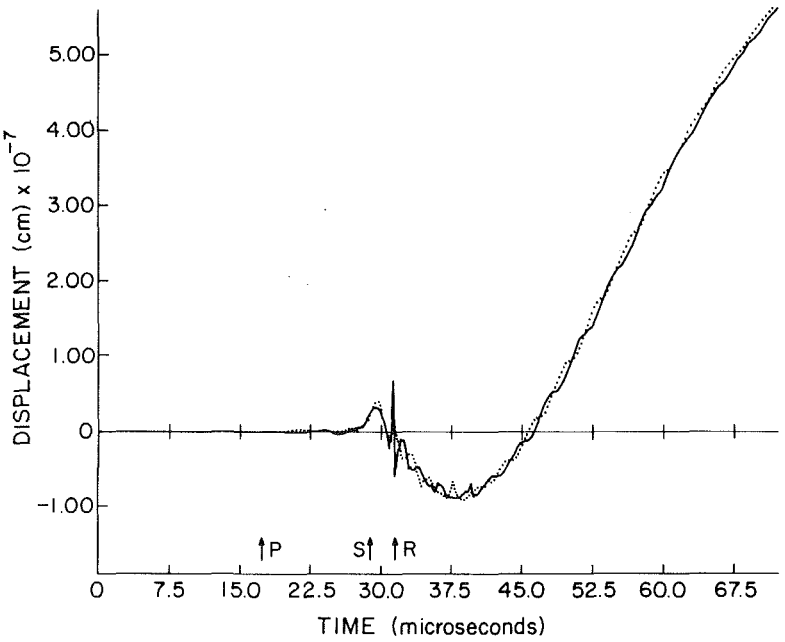

Fig. 8(*a*) The long time response at upper ($z = h$) and lower surface ($z = -h$)

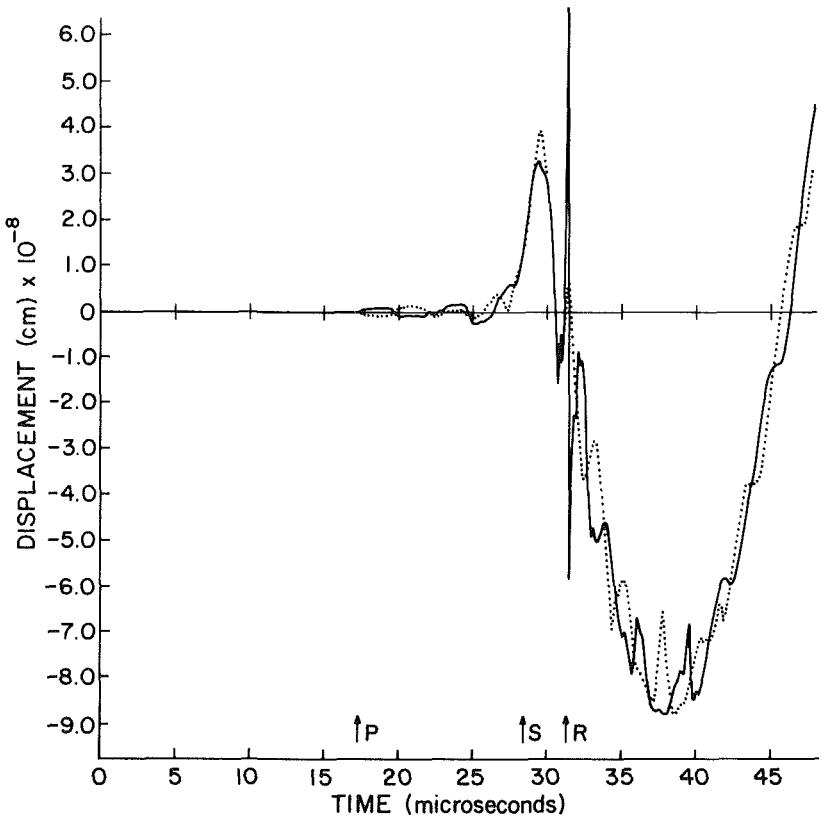

Fig. 8(*b*) Early time response in expanded scale

Fig. 8 Vertical displacements at the surfaces of the plate, solid line for $z = h$, dotted line for $z = -h$ ($r = 10$ cm)

The ensuing plots are the calculated vertical displacement responses of the surface of a glass plate due to an excitation of a step vertical downward force of 352 g; that is $Q_0 = -3.46$ N in equation (6.5),

$$\mathbf{F} = -346{,}000 \text{ (dynes)}\hat{\mathbf{z}}\,\delta(r)\delta(z-h)H(t)/2\pi r.$$

The glass has Poisson ratio 0.21 which is calculated from a shear wave speed $c_s = 0.349$ cm/μsec and a pressure wave speed $c_p = 0.576$ cm/μsec. Material density is 2.3 g/cm^3, and thickness of the plate is 0.96 cm. The values of these parameters were chosen to match the parameters of experimental work being done by Sachse and Pao [25].

8.1 Contributions From Individual Branches. In Figs. 6 and 7 we show u_{zm} (r, h, t) of equation (7.3) at a distance of 10 cm on the top surface of the plate ($z = h$) due to some of the lower branches. These plots can be qualitatively understood by the stationary phase analysis of the preceding section.

Downloaded From: https://appliedmechanics.asmedigitalcollection.asme.org on 06/27/2019 Terms of Use: http://www.asme.org/about-asme/terms-of-use

One clearly distinguishes, for instance, three major features in Fig. 6(*a*), the contribution of the first symmetric branch ($m=2$). One feature is the early arrival of a relatively low-amplitude and low-frequency component. The next feature is the sharp spike of very high frequency arriving at about 31 μsec. Finally there is, in the neighborhood of 60 μsec, an apparently exponentially decaying harmonic wave of a single frequency.

The plot of group velocity versus frequency for the first symmetric branch (Fig. 3(*a*)) shows three stationary points. The first is at a large group velocity $c_g \cong c_p$ and at low frequency. Associated with the point is a very low value for the modal factor (Fig. 5(*b*)). A group moving at this speed would arrive at $t = 18.0$ μsec in Fig. 6(*a*) (marked by $(S_1)_{max}$). There is also a local maximum at infinite frequency, with $c_g = c_R = 0.319$ cm/μsec associated with a nonzero modal factor. This occurs at R in Fig. 6(*a*) as the sharp Rayleigh peak ($t = 31.4$ μsec). Technically this peak ought to be of infinite height. A high-frequency cutoff in the numerical work where the modal factor Z has been set smoothly to zero above 2 MHz, has eliminated the singularity. Finally there is a minimum in the group velocity at a moderate frequency. Thus one expects and finds a late contribution Airy phase like that in Figure 4(*b*), tailing off at the point $(S_1)_{min}$ in Fig. 6(*a*) at $t = 58.0$ μsec. Each of these features is qualitatively predictable by the methods of Section 7.

The plot of displacement of the second symmetric branch S_2 in Fig. 6(*b*) also shows three major features. One is a nearly

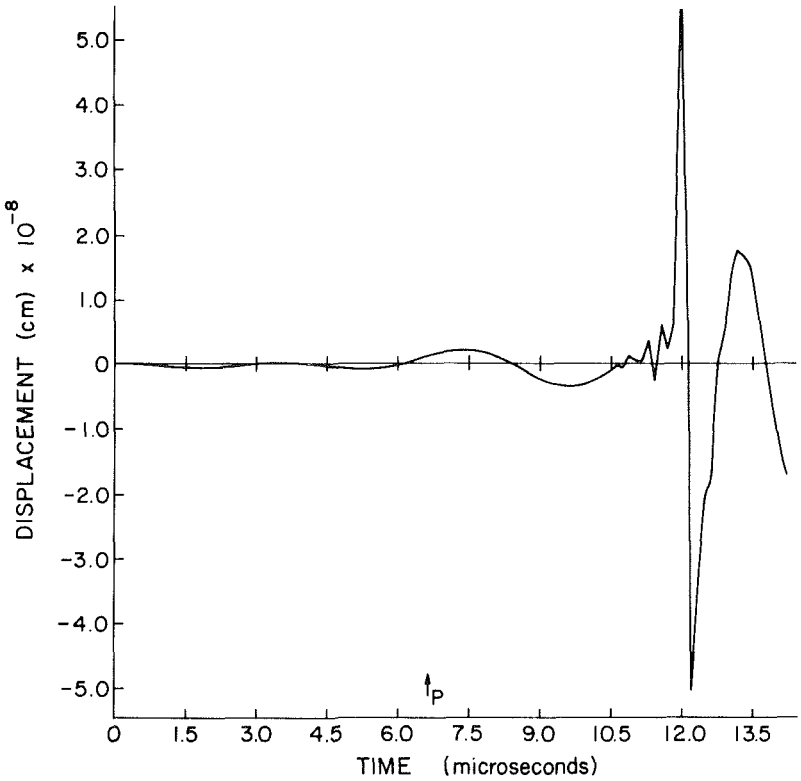

Fig. 9(*a*) Noncasual behavior due to the first symmetric branch

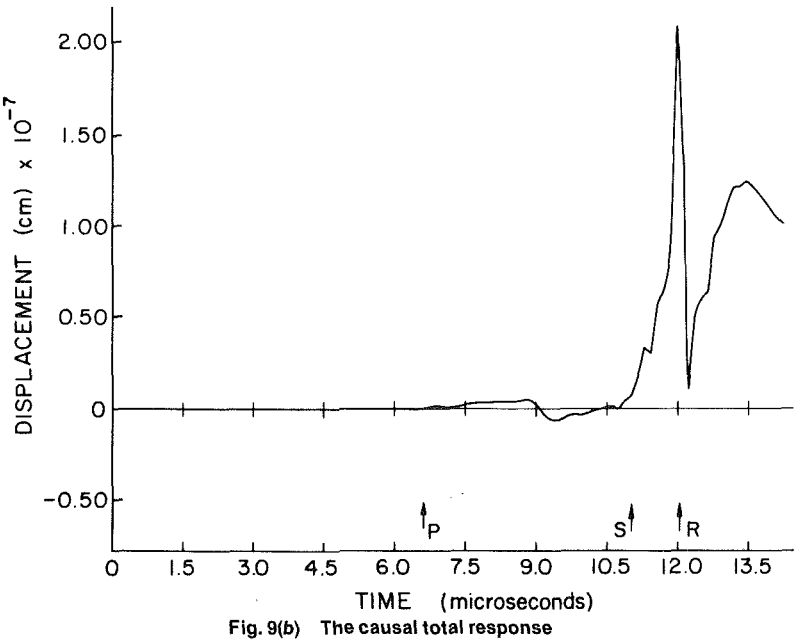

Fig. 9(*b*) The causal total response

Downloaded From: https://appliedmechanics.asmedigitalcollection.asme.org on 06/27/2019 Terms of Use: http://www.asme.org/about-asme/terms-of-use

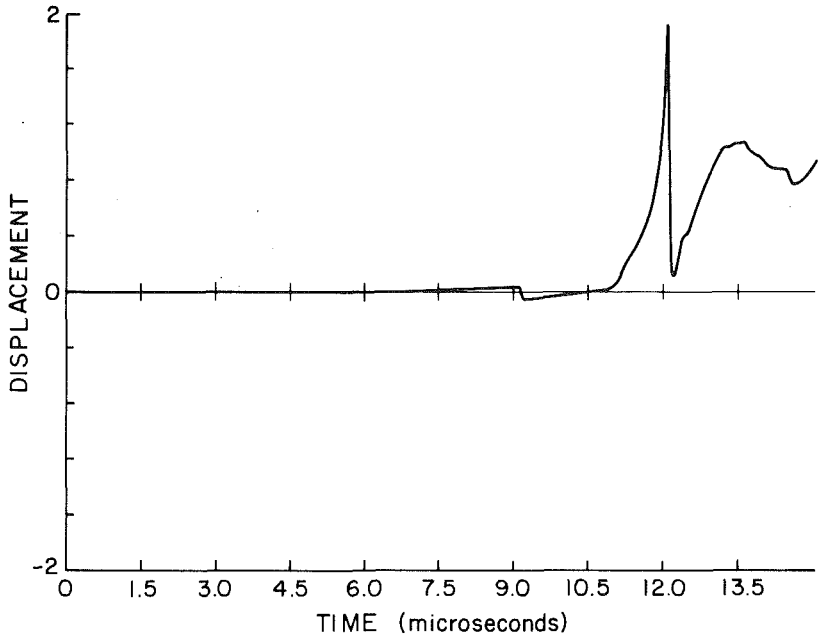

Fig. 9(c) Exact result of generalized ray theory

Fig. 9 Normal displacement at the upper surface of the plate ($r = 8h$)

constant frequency, very late large-amplitude component. Another is a high-frequency component confined to the times 30 μsec–43 μsec. The third is an early arrival of relatively low amplitude. These features also can be understood by considering the group velocity curve in Fig. 3(b) and the modal factor in Fig. 5(b). The long time scale ringing for instance is due to the large amplitude, low group velocity region near the cutoff frequency at $\kappa = 0$, and $\omega = 1.65\ \omega_s$.

The results shown in Fig. 6(c) for the third symmetrical branch, S_3, are similar to those of S_2.

The lowest antisymmetric branch (Fig. 7(a)) is of particular interest. It also has three main features. The first is a moderately low-frequency arrival approximately at the shear wave speed. There is also a sharp peak at the Rayleigh speed much like the same peak in Fig. 6(a). Finally there is an extremely low-frequency high-amplitude disturbance at late times. The sharp peak marked by R is a Rayleigh wave corresponding to the high-frequency asymptotic minimum in the group velocity. The early arrival is due to the sole maximum in group velocity at $(c_g)_{\max} = 0.996\ c_s$. The very large amplitude low-velocity disturbance corresponds to modes for which the group velocity is not stationary but for which the modal factor is immense. This is the low-frequency regime of flexural motion where the Germain-Lagrange bending theory would be valid [26].

Wave motion contributed by the second antisymmetric branch (A_2, $m = 3$) is shown in Fig. 7(b). Its features can be interpreted, as in the case for S_2, by the group velocity curve in Fig. 3(a) and modal factor curve in Fig. 5(a). The arrival times of various Airy phases $(A_2)_{\max}$, $(A_2)_{\min}$, and the arrival time of a shear ray are marked on the figure.

8.2 Normal Displacement at 10 Centimeters. Finally, in Figs. 8(a) and 8(b) we show the vertical displacement at 10 cm on the top at $z = h$ (solid lines), and on the bottom at $z = -h$ (dotted lines). The sum in equation (5.9) has been truncated at the first 10 branches (m from 1–10), thus fairly accurately including effects up to a frequency of the cutoff for the 11th branch ($\omega = 6\omega_s$, $f = 1.09$ MHz). As the modal factors appear to be dropping steadily with increasing order of branches, the indicated "total" displacement can be expected to be fairly good even above 1.09 MHz.

The upward displacement on top is of course the sum of contributions from each of the 10 branches at $z = h$ as discussed in the preceding subsection. The upward displacement at $z = -h$ is the sum of all the antisymmetric contributions at $z = h$ *minus* the sum of all the symmetric contributions at $z = h$. Thus, amongst other effects, the sharp Rayleigh wave peak due to the symmetric and antisymmetric lowest branches appears on the top surface, but does not appear on the bottom surface. To show the details of the Rayleigh arrival, the early time response at both surfaces are enlarged in Fig. 8(b).

8.3 Comparison With Response Based on Generalized Ray Theory. A particularly interesting phenomenon is exhibited in Fig. 9(a) for normal displacement at $r = 8h = 3.84$ cm due to the first symmetric branch. The response due to this branch alone is noncasual in the sense that there is disturbance before the arrival time of the P ray at 6.67 μsec. Similar noncausal behavior also exists for higher symmetric branches. One is thus suspicious of numerical error. The noncausal result for individual branches is, however, real, because the total response from all branches can still be causal (Fig. 9(b)).

Within the resolution of the numerical data, the noncausal parts of the second, third, and to a lesser extent, the higher symmetric branches have destructively interferred with those of the first branch, resulting in a correct result with zero response before the arrival of the P-wave. The sum of the contributions from the first 10 branches, a causal response, is shown in Fig. 9(b). The noncausal behavior for individual branches is also present at $r = 10$ cm but is much less pronounced there. The noncausual results, though initially surprising, cause no conceptual difficulties since a "branch" as discussed in Section 2 is not a concept fundamental to the plate response. It is impossible in principle to either excite or build a receiver receptive to only modes on a given branch. Similar results are reported in a treatment of elastic wave scattering (section 8.3, reference [4]).

In Fig. 9(c) we also show the exact result based on the generalized ray theory [11]. Its agreement with the result of normal mode theory appears good except for frequency components of the order of a megahertz or higher, as expected.

8.4 Response at 80h. The total surface response at $r = 80\ h$

Downloaded From: https://appliedmechanics.asmedigitalcollection.asme.org on 06/27/2019 Terms of Use: http://www.asme.org/about-asme/terms-of-use

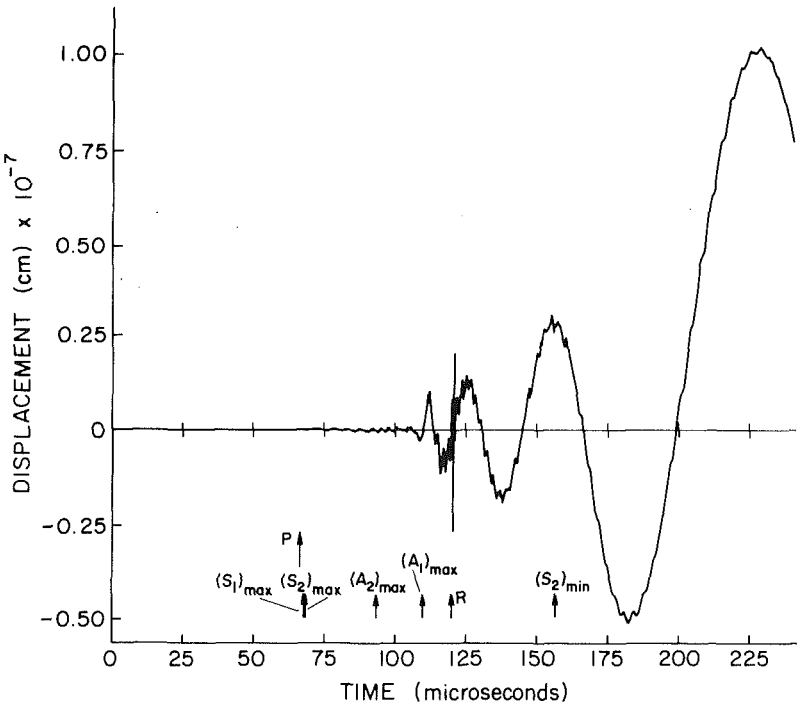

Fig. 10(*a*) Surface response at $r = 80\,h$

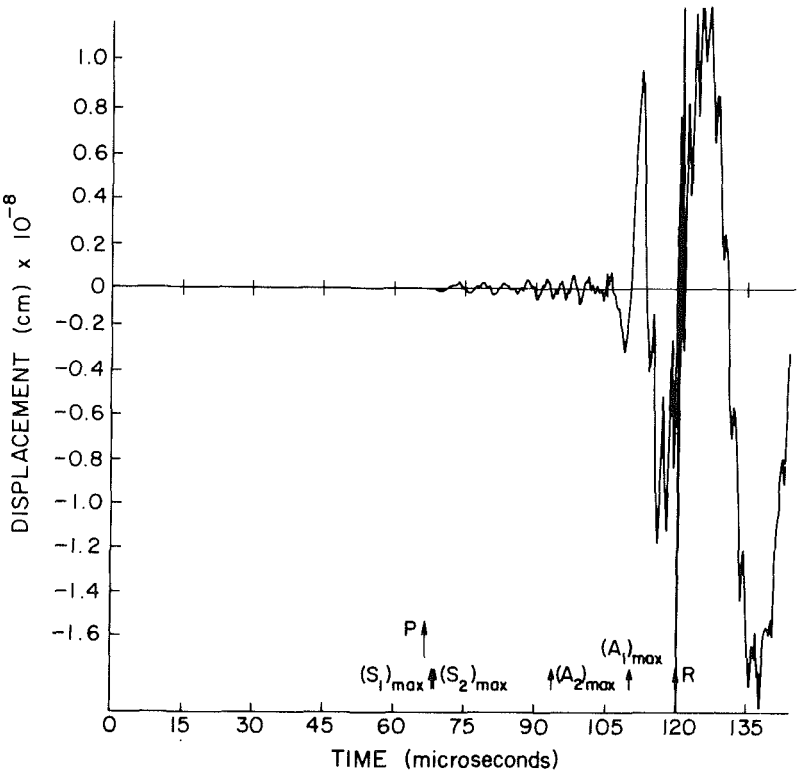

Fig. 10(*b*) Normal displacement at $z = +h$ in expanded scale

Fig. 10 Surface response at $r = 80\,h$

is calculated from a sum of 10 branches and is shown in Figs. 10(*a*) and 10(*b*). The distance is in the "intermediate range" ($20\,h < r < 200\,h$), and some of the features of the group velocity analysis should be identifiable. The arrival times of Airy phases traveling at some of the maximal and minimal group velocities are marked in the figure.

The early part of the displacement at $z = +h$ of Fig. 10(*a*) is shown enlarged in Fig. 10(*b*). In both figures, the modes of $(S_1)_{max}$ and $(S_2)_{max}$ are, however, not clearly present because the corresponding modal factors are nearly zero. The late arriving groups such as $(S_2)_{min}$, and the groups near the branch cutoff frequencies, such as the part responsible for the long time-scale ringing in Fig. 6(*b*), are somewhat masked in Fig. 10(*a*) by the large-amplitude, low-velocity, low-frequency, simple flexural response of the first antisymmetric branch. The presence of the higher frequency late-arriving groups would be more apparent in the output of a transducer with poor low-frequency response. There the group arrivals

Downloaded From: https://appliedmechanics.asmedigitalcollection.asme.org on 06/27/2019 Terms of Use: http://www.asme.org/about-asme/terms-of-use

would be somewhat more obvious, as would the long time-scale ringing, due predominently to the cutoff frequency domain of the second symmetric branch.

Comparison of these results with experimental results is problematic. Presently available experimental responses at large distances and long times are complicated by the presence of an unknown transducer transfer function [27]. Thus the voltage output of a pizoelectric transducer should not be compared directly with the displacement curves given here. Nevertheless a comparison has been made and the differences reasonably explained by some unknown linear transducer transfer function. Further work along these lines is ongoing.

9 Conclusion

In this paper, we have applied the method of expansion in normal modes to the solution of transient excitation of a thick plate, first to a plate with finite radius, then to an unbounded plate. The method of normal modes is chosen instead of the usual method of integral transform because it treats a buried force or moving force as easily as a surface force.

The final results for plate displacement are expressed as a series of integrals, each being integrated over the radial wave numbers of one branch of the Rayleigh-Lamb spectrum. These integrals are evaluated numerically up through the tenth branch.

Numerical results for the surface response of a plate at 10.42, 4, and 40 plate thickness from the source are shown in Figs. 8, 9(*b*), and 10, respectively, the source being a vertical force suddenly applied at the surface of the plate. Some features of these responses are interpreted in terms of a stationary phase analysis and the group velocities of Rayleigh-Lamb waves in the plate. Within the very large present experimental uncertainties, the result at 40 plate thickness is in agreement with the experimental measurement. The result at 4 plate thicknesses agrees very well with the exact results derived from the theory of generalized ray. We conclude that the method of normal modes can be applied effectively to analyze transient progressive waves in a plate at intermediate and far range.

Acknowledgment

The authors acknowledge the support provided by the National Science Foundaton through a grant to the College of Engineering (ENG 7910311), and one to the Materials Science Center of Cornell University.

References

1 Lord Rayleigh, "On the Free Vibrations of an Infinite Plate of Homogeneous Isotropic Elastic Matter," *Proceedings London Mathematical Society*, Vol. 20, 1888–1889, p. 225.

2 Lamb, H., "On Waves in an Elastic Plate," *Proceedings Royal Society London*, Series A, Vol. 93, 1916–1917, p. 114.

3 Mindlin, R. D., "Waves and Vibrations in Isotropic, Elastic Plates," in: *Structural Mechanics*, Goodier, J. N., and Hoff, N. J., Eds., Pergamon Press, New York, 1960.

4 Miklowitz, J., *The Theory of Elastic Waves and Wave Guides*, North-Holland, Amsterdam, 1978.

5 Lloyd, J. R., and Miklowitz, J., "On the Use of Double Integral Transforms in the Study of Dispersive Elastic Wave Propagation," *Proceedings of the Fourth U.S. National Congress of Applied Mechanics*, Vol. 1, The American Society of Mechanical Engineers, New York, 1962, pp. 255–267.

6 Miklowitz, J., "Transient Compressional Waves in an Infinite Elastic Plate or Elastic Layer Overlying a Rigid Half-Space," ASME JOURNAL OF APPLIED MECHANICS, Vol. 29, 1962, pp. 53–60.

7 Scott, R. A., and Miklowitz, J., "Transient Nonaxisymmetric Wave Propagation in an Infinite Isotropic Elastic Plate," *International Journal of Solids and Structures*, Vol. 5, 1969, pp. 65–79.

8 Mencher, A. G., "Epicentral Displacement Caused by Elastic Waves in an Infinite Slab," *Journal of Applied Physics*, Vol. 24, 1953, pp. 1240–1246.

9 Knopoff, L., "Surface Motions of a Thick Plate," *Journal of Applied Physics*, Vol. 29, 1958, pp. 661–670.

10 Davids, N., "Transient Analysis of Stress-Wave Penetration in Plates," ASME JOURNAL OF APPLIED MECHANICS, Vol. 26, 1959, p. 651.

11 Pao, Y. H., Gajewski, R. R., and Ceranoglu, A. N., "Acoustic Emission and Transient Waves in an Elastic Plate," *Journal of the Acoustical Society of America*, Vol. 65, 1979, pp. 96–105.

12 Ceranoglu, A. N., and Pao, Y. H., "Propagation of Elastic Pulses and Acoustic Emission in a Plate, Part I. Theory, Part II. Epicentral Response, Part III. General Responses," ASME JOURNAL OF APPLIED MECHANICS, 1981, pp. 125–147.

13 Love, A. E. H., *Mathematical Theory of Elasticity*, 4th ed., Dover, New York, 1944.

14 Eringen, A. C., and Suhubi, E. S., *Elastodynamics, Vol. 2, Linear Theory*, Academic Press, New York, 1975.

15 Reismann, H., "On the Forced Motion of Elastic Solids," *Appl. Sci. Res.*, Vol. 18, 1967, p. 156.

16 Goodman, L. E., "Circular Crested Vibrations of an Elastic Solid Bounded by Two Parallel Planes," *Proceedings of First U.S. National Congress of Applied Mechanics*, The American Society of Mechanical Engineers, New York, 1951, p. 65.

17 Meeker, T. R., and Meitzler, A. H., "Guided Wave Propagation in Elongated Cylinders and Plates," in: *Physical Acoustics*, Vol. 1A, Mason, W. P., Ed., Academic Press, New York, 1964, pp. 111–167.

18 Pao, Y. H., and Kaul, R. K., "Waves and Vibrations in Isotropic and Anisotropic Plates," in: *R.D. Mindlin and Applied Mechanics*, Herrmann, G., Ed., Pergamon Press, New York, 1974.

19 Hutchinson, J. R., "Vibrations of Solid Cylinders," ASME JOURNAL OF APPLIED MECHANICS, Vol. 47, 1980, pp. 901–907.

20 National Bureau of Standards, *Handbook of Mathematical Functions*, Abramowitz, M., and Stegun, I. A., Eds., U.S. Government Printing Office, Washington, D.C., 1964.

21 Pursey, H., "The Launching and Propagation of Elastic Waves in Plates," *The Quarterly Journal of Mechanics and Applied Mathematics*, Vol. 10, 1957, p. 45.

22 Copson, E. T., *Asymptotic Expansions*, Cambridge University Press, Chapter 4, 1965.

23 Chester, C., Friedman, B., and Ursell, F., "An Extension of the Method of Steepest Descent," *Proceedings Cambridge Philosophical Society*, Vol. 53, 1957, p. 599.

24 Longman, I. M., "Note on a Method for Computing Infinite Integrals of Oscillating Functions," *Proceedings Cambridge Philosophical Society*, Vol. 52, 1956, p. 764.

25 Sachse, W., and Pao, Y. H., "Propagation of Wide Band Pulses in an Elastic Plate," in preparation.

26 Medick, M., "On Classical Plate Theory and Wave Propagation," ASME JOURNAL OF APPLIED MECHANICS, Vol. 28, 1961, p. 223.

27 Sachse, W., and Hsu, C. S., "Ultrasonic Transducers for Materials Testing and Their Characterization," in: *Physical Acoustics*, Vol. 14, Mason, W. P., and Thurston, R. N., Eds., Academic Press, New York, 1979, pp. 277–406.

Downloaded From: https://appliedmechanics.asmedigitalcollection.asme.org on 06/27/2019 Terms of Use: http://www.asme.org/about-asme/terms-of-use